Monthly Notices
of the
ROYAL ASTRONOMICAL SOCIETY

MNRAS **471,** 355–363 (2017)
Advance Access publication 2017 June 22

doi:10.1093/mnras/stx1575

Orbital variations in intensity and spectral properties of the highly obscured sgHMXB IGR J16318−4848

Nirmal Iyer★† and Biswajit Paul★

Raman Research Institute, Bangalore 560080, India

Accepted 2017 June 20. Received 2017 June 20; in original form 2017 April 27

ABSTRACT

IGR J16318−4848 is an X-ray binary with the highest known line-of-sight absorption column density among all known X-ray binary systems in our Galaxy. In order to investigate the reason behind such a large absorption column, we looked at the variations in the X-ray intensity and spectral parameters as a function of the tentatively discovered ∼80 d orbit of this source. The orbital period is firmly confirmed in the long-term (∼12 yr) *Swift* BAT light curve. Two peaks about half an orbit apart, one narrow and small, and the other broad and large, are seen in the orbital intensity profile. We find that while most orbits show enhanced emissions at these two peaks, the larger peak in the folded long-term light curve is more a result of randomly occurring large flares spread over ∼0.2 orbital phase. As opposed to this, the smaller peak is seen in every orbit as a regular increase in intensity. Using archival data spread over different phases of the orbit and the geometry of the system as known from previously published infrared observations, we present a possible scenario that explains the orbital intensity profile, flaring characteristics and large column density of this X-ray binary.

Key words: X-rays: binaries – X-rays: individual: IGR J16318−4848.

1 INTRODUCTION

Hard X-ray surveys with the coded mask imagers on *INTEGRAL* and *Swift* observatories have revealed a class of highly obscured supergiant high-mass X-ray binary (sgHMXB) systems in the Galactic plane. These binaries are characterized by persistently high line-of-sight absorption column ($N_{\rm H} > 10^{23}$ cm^{-2}) as inferred from their X-ray spectrum. Most of these sources are thought to be classical sgHMXBs undergoing transition to Roche lobe overflow, with low wind velocities (Walter et al. 2015). However, exceptions to such an explanation are seen in the case of IGR J16320−4751 (with an 8.9 d orbit) and CI Cam (with a 19.4 d orbit). Such a large orbit makes it unlikely for these systems to be Roche lobe transiting systems. IGR J16320−4751 is seen to have significantly larger infrared reddening than expected from the column estimated via 21-cm H I line surveys, indicating that this system has a large amount of dust present in the vicinity of the source (Chaty et al. 2008; Walter et al. 2015). CI Cam too is thought to have the presence of an enshrouding dust shell surrounding the compact object (Bartlett et al. 2013). The discovery of an 80 d orbit of IGR J16318−4848 (Jain, Paul & Dutta 2009), an X-ray binary with the highest known persistent absorption column ($N_{\rm H} \sim 10^{24}$ cm^{-2}; Ibarra et al. 2007) added another interesting exception to this list.

IGR J16318−4848 was first discovered in 2003 by the IBIS/ISGRI onboard *INTEGRAL* (Courvoisier et al. 2003). It was quickly revealed that this source had an exceptionally high absorption column and very prominent iron and nickel fluorescence lines in X-rays (Matt & Guainazzi 2003). The source was also seen to display large variations in its X-ray intensity over time-scales of kiloseconds to days (Courvoisier et al. 2003; Krimm et al. 2010). Infrared observations post-*XMM* localization of the source position led to the identification of a possible sgB[e] counterpart with a high intrinsic absorption and a complex and dense circumstellar medium surrounding the companion star (Filliatre & Chaty 2004). Further spectroscopic observations in the mid-infrared indicated the presence of a large (∼5.6 au) dusty viscous disc surrounding the sgB[e] star in which the compact object is possibly enshrouded, thereby giving the high $N_{\rm H}$ (Chaty & Rahoui 2012).

Indications of an orbital periodicity in the *Swift* BAT light curve were reported in 2009 by Jain et al. (2009). The authors found a periodicity of ∼80 d and a single large peak in the orbital intensity profile along with smaller secondary peaks. However, no periodicities or pulsations at smaller time-scales have been reported for this source, despite the fact that multiple searches have been made using data from different observatories (Walter et al. 2003; Barragán et al. 2009).

We investigated persistence of the orbital intensity modulation and the source's flaring nature with additional data from *Swift* BAT and *INTEGRAL* ISGRI. We also examined archival data from the *XMM–Newton*, *Swift*, *NuSTAR* and *ASCA* observatories to search for pulsations and to check for orbit-phase-dependent variations

★ E-mail: nirmal.iyer@gmail.com (NI); bpaul@rri.res.in (BP)
† NI present address : Albanova University Center, KTH, Stockholm 106 91, Sweden.

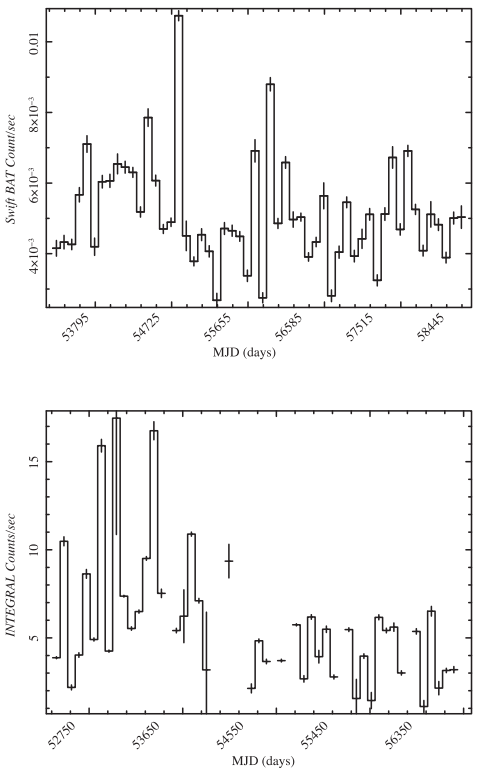

Figure 1. Light curves from *Swift* BAT (top panel) and *INTEGRAL* ISGRI (bottom panel) binned at $\sim 7 \times 10^6$ s. *INTEGRAL* has lot of gaps in the data as compared to *Swift* BAT.

in the spectrum. We present the results of this investigation in the following sections. In Section 2, we summarize the observations used and the steps we followed to reduce the data from various observatories. We also list the main results that we obtained in this section. In Section 3, we discuss the relevance of these results and try to piece together an overall picture of the binary system.

2 OBSERVATIONS AND ANALYSIS

In order to examine the intensity variations in this source, we divided our analysis into two parts. The first part relates to the long-term monitoring observations and the second part relates to individual pointed mode observations. The long-term data was obtained from two sources. These were the 1 d averaged light curve of *Swift* BAT[1] and the pre-reduced 1 h bin-size light curves from *INTEGRAL* ISGRI.[2] These two light curves are shown in Fig. 1 with a bin-size equal to the orbital period (discussed later).

The pointed observations were obtained from the HEASARC data archive.[3] Table 1 lists these observations. As the archival pointed observations were not targeted at studying variations with the orbital phase, we find that certain orbital phases are not covered. As we note later, the absence of pointed observations in some orbital phases limits the conclusions we can draw from these observations.

The pointed mode observations were reduced using the standard observatory pipelines made available by each of the X-ray observatories. Data from the EPIC-pn instrument onboard *XMM–Newton* was used for extracting spectral information. This was done using the *XMM* software suite SAS v15.0.0, with standard reduction techniques as specified in the *XMM*-SAS user guide.[4]

We used data from both the focal plane modules (FPMA and FPMB) of the *NuSTAR* observatory. In order to reduce *NuSTAR* data, the software tools `nuproducts` and `nupipeline` were used from the software suite HEASOFT v6.20. The calibration files for *NuSTAR* were updated till 2017 Jan. The data reduction was done as per the instructions in the NuSTAR data analysis software user guide.[5] We also made use of data from the XRT instrument onboard *Swift*, XIS and PIN instruments onboard *Suzaku* and GIS instrument onboard *ASCA* to obtain the X-ray spectrum. The data reduction for these instruments was also done using tools provided in the HEASOFT v6.20 package with calibration files updated till 2017 Jan. To fit the spectrum obtained from the reduced data, we used XSPEC, a spectral fitting software package in HEASOFT.

2.1 Long-term observations

We checked for signatures of the orbital modulation in both the *INTEGRAL* ISGRI and *Swift* BAT light curves. We used both the daily averaged (DA) and the satellite orbit averaged (SOA) light curves from BAT for this analysis. However, the BAT imaging process can cause additional systematic errors to be present in the data due to multiple possible reasons (see Krimm et al. 2013, for details). Before carrying out a detailed analysis, we excluded data with error bars larger than 10^3 times the minimum error value in the BAT light curve.

We searched for signatures of an orbital period in the BAT DA light curves and in the ISGRI light curves. This was done by using the tool `efsearch` on the long-term light curves. `efsearch` searches for periodicity by folding the light curve at different test periods and comparing the folded profile against a constant non-varying profile (Leahy et al. 1983). Given the previous detection of an orbital period at ∼80 d, we searched for a periodicity in the period range from 60 to 100 d. The results so obtained are shown in Fig. 2. As seen in the figure, there is a clear signature of periodicity in both the light curves at ∼80 d. Since the *INTEGRAL* data has multiple long data gaps (100–500 d) between two stares of the Galactic Centre region, where this source resides, the periodicity in ISGRI light curve is not as significant as in the BAT light curve. The strong signature of periodicity in the BAT light curve and an indication of a periodicity at the same period in the *INTEGRAL* light curve confirms the periodicity reported in Jain et al. (2009) and marks it as an orbital period. This period of ∼80 d is the highest reported orbital period in the small sample of highly obscured sgHMXBs that are known currently. For all further analysis, we used the period detected with *Swift* BAT at 80.09 ± 0.012 d.

The orbital period folded profile with folding epoch taken at MJD 53477.577 and 32 phase bins per period is shown in Fig. 3. The epoch for folding is taken such that the highest intensity appears at orbital phase 0.5. From the figure, it is clear that the intensity goes high in two phase sections of the orbit, namely the phase between 0.10 and 0.25 and the phase between 0.35 and 0.65. Now on, we shall refer to the brightest section as the Main Peak, the smaller hump as the Secondary Peak and the rest as low intensity phases, as is demarcated in Fig. 3. This enables us to examine the characteristics

[1] https://swift.gsfc.nasa.gov/results/transients/
[2] http://www.isdc.unige.ch/integral/heavens
[3] https://heasarc.gsfc.nasa.gov/docs/archive.html
[4] http://xmm-tools.cosmos.esa.int/external/xmm_user_support/documentation/sas_usg/USG/SASUSG.html
[5] http://heasarc.gsfc.nasa.gov/docs/nustar/analysis/nustar_swguide.pdf

Table 1. Archival pointed mode observations used for studying spectral variations with orbital phase.

Date (UTC)	Obs-id	Observatory	Orb. phase[a]	Exposure (ks)	Remarks
1994-09-03	92000180	*ASCA*	0.57	10.78	
2003-02-10	0154750401	*XMM–Newton*	0.05	26.98	
2004-02-18	0201000201	*XMM–Newton*	0.70	21.92	
2004-03-20	0201000301	*XMM–Newton*	0.10	25.52	
2004-08-20	0201000401	*XMM–Newton*	0.00	21.91	
2006-08-14	401094010	*Suzaku*	0.66	97.25	
2007-05-04	00035053003	*Swift*	0.32	6.9	Longest duration *Swift* observation with 57 photons in XRT
2014-08-22	0742270201	*XMM–Newton*	0.63	94.0	
2014-08-22	30001006002	*NuSTAR*	0.63	56.57	Taken simultaneously with *XMM* obs 0742270201

Note. [a]Reference epoch is MJD 53477.577 and period is 6920 742.0 s. Phase is of mid-observation. See the text for details.

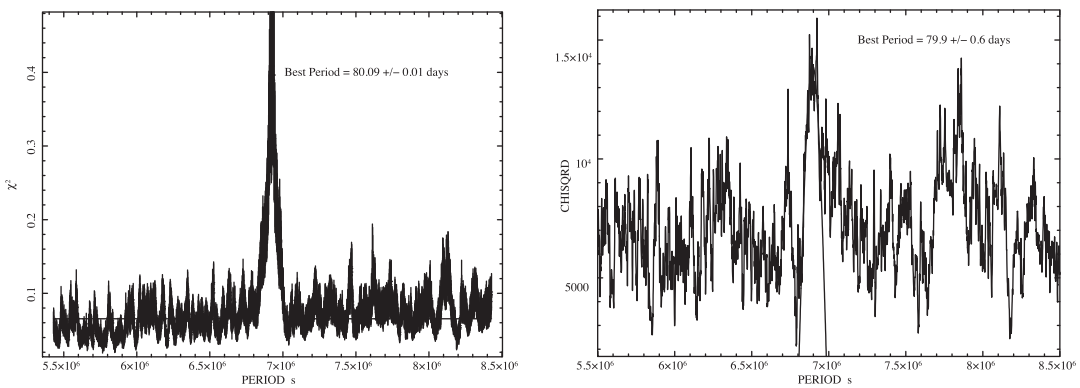

Figure 2. Results from the period search using *Swift* BAT light curve (left-hand panel) and *INTEGRAL* light curve (right-hand panel). Figure plotted without error bars for clarity. The most likely value of the period is found by fitting a Gaussian curve to the peak in chi-square distribution obtained from the period search.

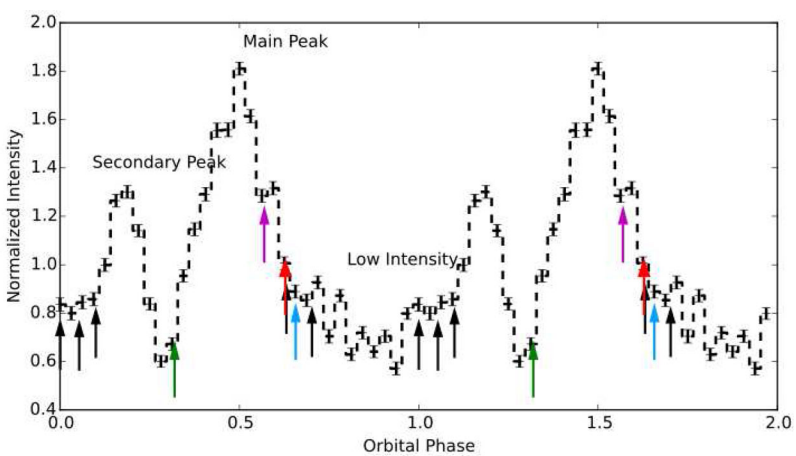

Figure 3. Orbital intensity profile as obtained from *Swift* BAT light curve showing orbital intensity modulations as a function of the orbital phase. The figure also shows the phase of each of the pointed mode observations with *XMM* in black, *Swift* in green, *NuSTAR* in red, *ASCA* in magenta and *Suzaku* in blue arrows. See online for a colour version of this figure.

of each of these phases separately in order to understand the reason behind such intensity variations.

To further examine this dual peaked intensity variation, we took a closer look at the long-term light curves and the X-ray spectra from each of the pointed mode observations. The results of these are described in Section 2.2.

2.1.1 Orbital timing analysis

In order to see if the two peaks are persistently present in all orbits or if they are a result of intermittent flares in some orbits (as was reported in a short duration of BAT light curves in Jain et al. 2009), we divided the long-term *Swift* BAT light curve into individual orbits (of 80.09 d). The BAT data obtained for ∼12 yr since 2005 gave us about 54 orbits for this source. Krimm et al. (2010) reported two of the consecutively seen flares from *Swift* BAT to be separated by three times the reported orbital period. We examined the data closely to see if such orbital phase dependence of flares was true for all flares.

Using the same criteria as in Krimm et al. (2010), viz. flux greater than 130 mCrab (0.029 cts s^{-1} cm^{-2}) and significance greater than 10, we picked all data points that can be classified

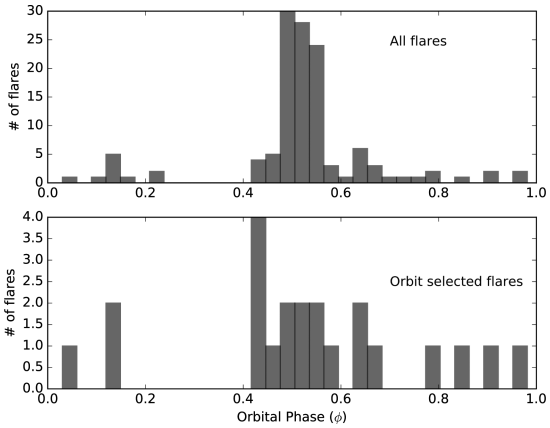

Figure 4. Phase distribution of flares in the orbit. Top panel shows the orbital phase of all flares. Bottom panel shows orbit-selected flares. See the text for details.

to be flaring in the BAT SOA data. In addition, we used the conditions `DATA_FLAG == 0` and `DITHER_FLAG == 0` (see footnote 1). Of the ∼50 000 points in the SOA data, only 77 points were seen to satisfy this criteria. If we relax the condition for dithering to be present, we get 124 data points. Since this analysis was done on the SOA data, where contributions to the systematic error due to non-dithering mode observations are relatively less, we consider all 124 data points to be valid flares.

Using the same orbital period and epoch used to fold the BAT light curves, we tried to see the orbital phase at which the flares occur. Fig. 4 shows the phase distribution of these flares. As is immediately evident from this figure, most (99 of 124) of the flares occur in the phase corresponding to the Main Peak. We also note that quite a few (8) flares exist in the phase that corresponds to the Secondary Peak. It is to be noted that a majority (64) of the points in flares in the Main Peak belong to one outburst (consisting of multiple consecutive flaring points) in 2008 September, as seen in the left-hand panel of Fig. 5. We checked to see if all other flares happen in the Main Peak by observing orbit-selected flares.

This was done by taking only one representative point for every orbit by recording the phase of the flare with the highest flux in that orbit. Making a histogram of this (bottom panel of Fig. 4) still shows that a majority (13 of 22) of the orbits have flares in Main Peak. A further three points lie just after the Main Peak (0.65–0.8) and two points lie in the Secondary Peak. This accounts for 18 of 22 orbits showing flares, thereby indicating a strong orbital phase preference for these flares. However, it is interesting to note that a few orbits (4 of 22) show flares that are not in either of the two Peaks.

We tried to see if there is a recurrence rate to the occurrence of flares by noting the orbits in which the flares occurred. However, as plotted in the left-hand panel of Fig. 6, there seems to be no periodic pattern to the occurrence of these orbits. The only noticeable change

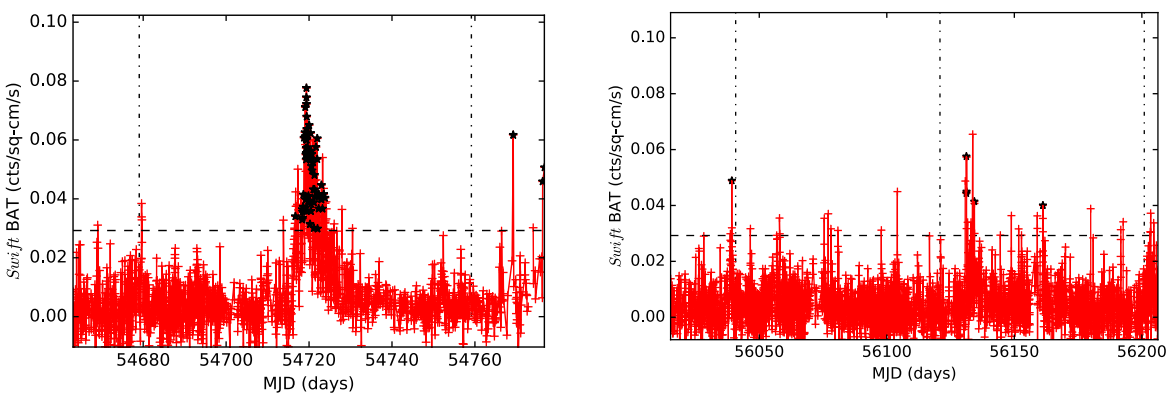

Figure 5. The BAT SOA light curve for a few orbits of data with flares detected in *Swift* BAT SOA. Left-hand panel shows flares in a major outburst in 2008. Right-hand panel shows some of the data points detected in the Secondary Peak in 2012. In both figures, the horizontal line corresponds to the 130 mCrab threshold and the vertical lines correspond to the ephemeris at phase zero of each orbit. SOA data points selected to be in a flaring state are marked in black. See online text for a colour version of this figure.

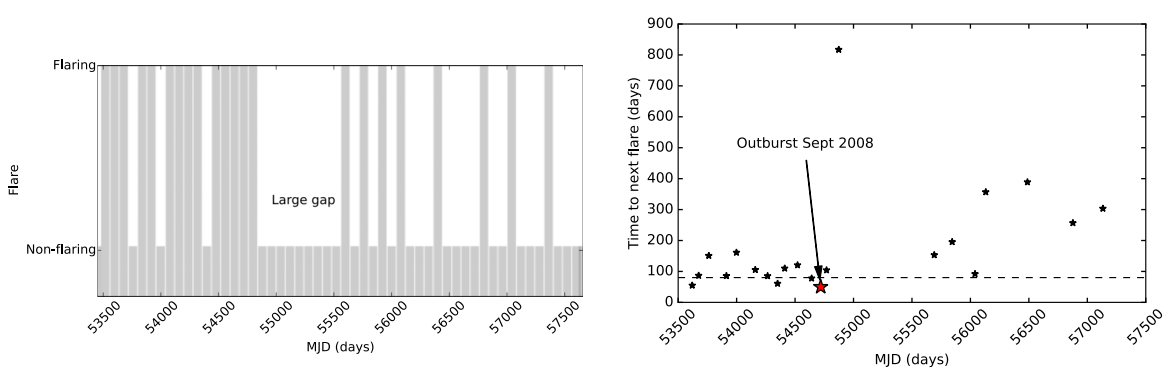

Figure 6. Left-hand panel shows orbits in which flares were detected. Almost every orbit had a detected flare before a large gap without flares was seen starting 2009 Feb (orbit number 18). Right-hand panel shows time to next flare. As seen after MJD 54890 (2009 Feb), the time to next flare shows a significant increase as compared to pre-2009 flares.

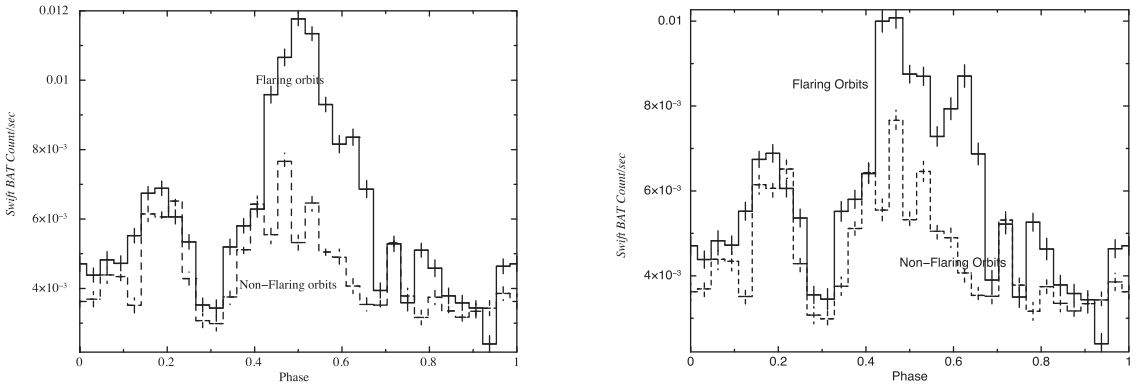

Figure 7. Comparison of the folded profiles of orbits with flaring observations to orbits without any flares. The right-hand panel constructs the folded profiles by ignoring data points from the large outburst of 2008 Sep.

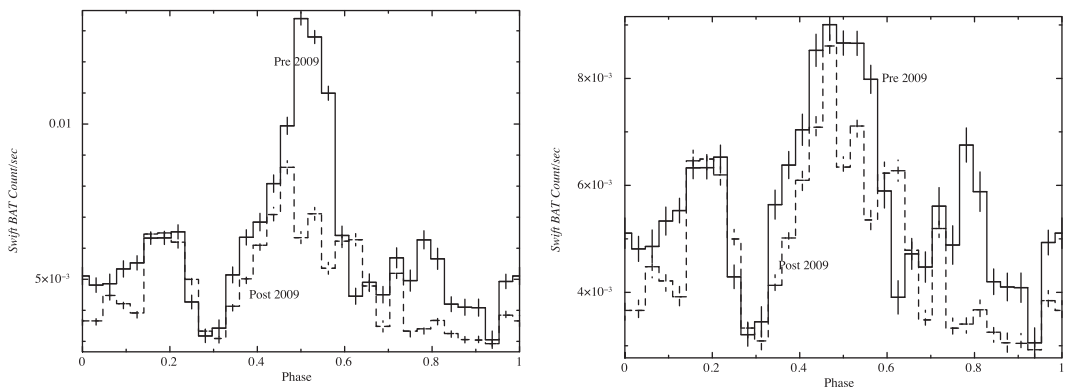

Figure 8. Comparison of the folded profile before the large gap starting 2009 Feb to the profile after the large gap. The right-hand panel constructs these profiles by ignoring data points from the large outburst of 2008 Sep.

seems to be the fact that the source was in a frequent flaring mode before 2009 Feb. This is also shown in the right-hand panel of Fig. 6 where the time to next flare is plotted. From these plots, we note that there is an ∼10 orbit gap after the detected flare in 2009 Feb. Post this large gap, the time to next flare shows a sporadic distribution, with values much larger than those before 2009 Feb. We note that in 2008 Sep, two orbits before the large gap with no flares, a major outburst is seen in the *Swift* BAT data (also see the left-hand panel of Fig. 5). This behaviour seems similar to disc-fed systems where the time to next outburst is directly proportional to the luminosity of the outburst, suggesting some kind of disruption and re-formation of the accreting material in the disc (see the case of dwarf novae as explained by the disc instability model in Osaki 1996, and references therein).

2.1.2 Orbit folded profiles

The orbital phase preference for occurrence of flares is seen in the previous section. However, the source light curves also seem to show the orbital modulation in the absence of flares. This is seen in Fig. 7. For making this figure, the 22 orbits that had at least one flaring observation were folded together and compared with the folded profile of the remaining 32 orbits that had no flaring observations. The figure indicates that non-flaring orbits also have enhanced emission at the phases corresponding to the Main and Secondary Peaks, with the folded amplitudes in these two peaks being comparable. However, flaring orbits seem to have a much higher amplitude in the Main Peak. We note that the large outburst of 2008 Sep biases these folded profiles. Therefore, we also compared the folded profiles by neglecting data from this outburst as seen in the right-hand panel of Fig. 7. The Main Peak continues to have a higher amplitude in the flaring orbits as compared to non-flaring orbits. This indicates that the preference for flares to occur in the phases corresponding to the Main Peak increases its amplitude as seen in the folded profile of the entire light curve, while the Secondary Peak corresponds to a phase of enhanced emission in almost all orbits.

We also tried to see if the folded profile changed before and after the large gap starting 2009 Feb. The light curves corresponding to these time periods were folded separately, with the resultant profiles plotted in Fig. 8. We folded these profiles with and without the outburst of 2008 Sep., similar to Fig. 7. We find that the folded profiles do not change much before and after the large gap (starting 2009 Feb) if the 2008 Sep. outburst is not considered.

2.2 Pointed observations

The pointed mode observations of IGR J16318−4848 show intensity variations over the course of a single observation (Matt & Guainazzi 2003). We tried to check if these variations too have any signatures of periodicity. We also examined how these variations differ across different X-ray energy bands. Finally, we checked to see how these short-term variations link with the orbital variations in the source. The following paragraphs detail the results of this investigation.

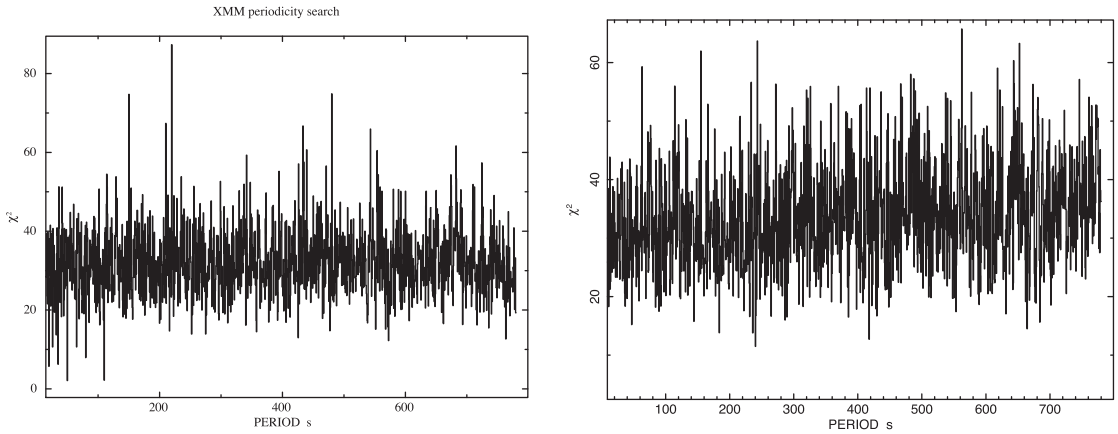

Figure 9. Results of pulsation search in *XMM* (left-hand panel) and *NuSTAR* (right-hand panel) data from 0.5 s to 1 ks. The non-detection of pulsations enabled us to put an upper limit of ∼1 per cent for *XMM* and ∼4 per cent for *NuSTAR* on the pulse fraction of any un-detected pulsation.

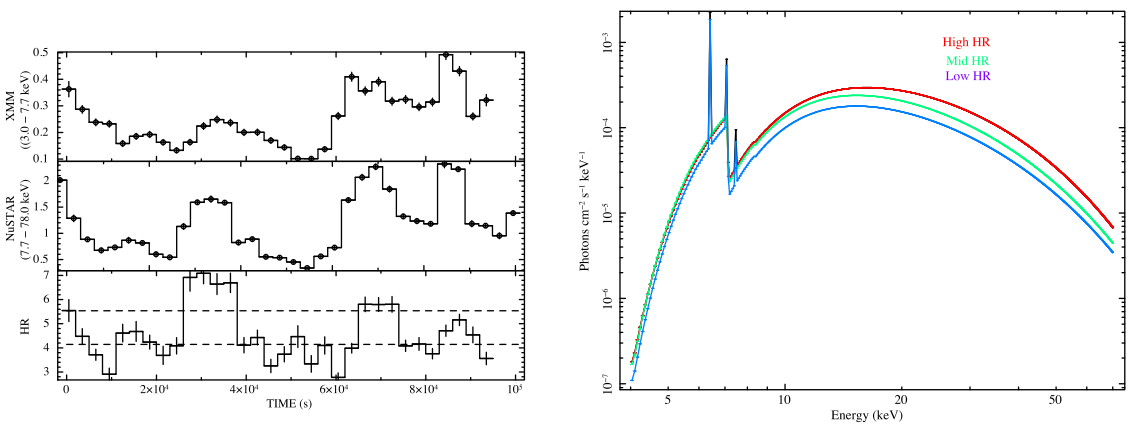

Figure 10. HR and spectral variations over a pointed observation. Left-hand panel shows HR variations and the *XMM* and *NuSTAR* light curves in the observation period. Horizontal lines show levels used to create the HR resolved spectra. Right-hand panel shows the best-fitting models indicating the spectral changes as a function of change in the HR value for three HR levels (red for high, green for mid and blue for low). See online text for a colour version of this figure.

2.2.1 *Search for pulsations*

Most HMXB systems have a neutron star as the compact object (see Casares et al. 2014, for an exception). Walter et al. (2003) reported absence of pulsations in IGR J16318−4848 using *XMM* observations, with a marginal signature of a quasi periodic oscillation (QPO) at 0.15 Hz. Barragán et al. (2009) noted that even the harder X-rays as seen by *Suzaku* gave no pulsation signatures in this source in the range from 1 s to 10 ks.

We searched for pulsations in the *NuSTAR* light curve and the simultaneously taken *XMM* light curve for pulsation signatures. This *XMM* data was taken in the small window mode, enabling a time resolution of 5.7 ms. The light curves for both *XMM* and *NuSTAR* were barycentred before the search was made. Fig. 9 shows the results of the period search. As seen in the figure, no pulsations are detected either in the soft (<10 keV) or hard (up to 70 keV) bands, with an upper limit on pulse fraction of ∼1 per cent in *XMM* and ∼4 per cent in *NuSTAR*. The QPO feature at ∼0.15 Hz was also not seen in the power density spectrum from these light curves. We do note that `efsearch` gives high χ^2 values for periods greater than 2000 s in both the *XMM* and *NuSTAR* data. We believe that this could be due to an inherent slow kilosecond scale variability in the source as pointed out in Section 2.2.2.

2.2.2 *Intensity and spectral variations at smaller time-scales – the* XMM – NuSTAR *simultaneous observation*

The source exhibits a significant variation of intensity over the course of a single pointed observation. The source intensity often changes by an order of magnitude over a few kiloseconds (see the first *XMM* observations reported in Matt & Guainazzi 2003). This variation is reflected in both the power density spectrum (with high power in the sub mHz region) and `efsearch` results.

We tried to see if these intensity variations over the course of a pointed observation lead to hardness ratio (HR) and spectral changes. The left-hand panel of Fig. 10 plots the light curves in the soft *XMM* (3.0–7.7 keV) and hard *NuSTAR* (7.7–78 keV) bands. The bands were chosen such that the line energies and the most of the continuum fall in separate bands. The variations in both these bands seem well correlated as indeed was observed by Matt & Guainazzi (2003) and Barragán et al. (2009). Matt & Guainazzi (2003) also noted little to no change in the spectral parameters (other than overall normalization) between the observations at different luminosity levels. The HR plot of the *Suzaku* instruments (fig. 5 of Barragán et al. 2009) shows changes in HR values over the *Suzaku* observation. However, it is difficult to comment on these changes and their relation to change in the X-ray flux. The HR plot obtained by the more sensitive observation using simultaneous stares by *XMM*

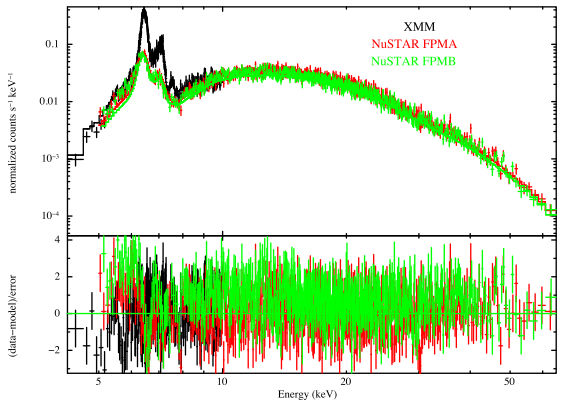

Figure 11. Spectrum averaged over entire *XMM-NuSTAR* simultaneous observation. See the text for details. See online text for a colour version of this figure.

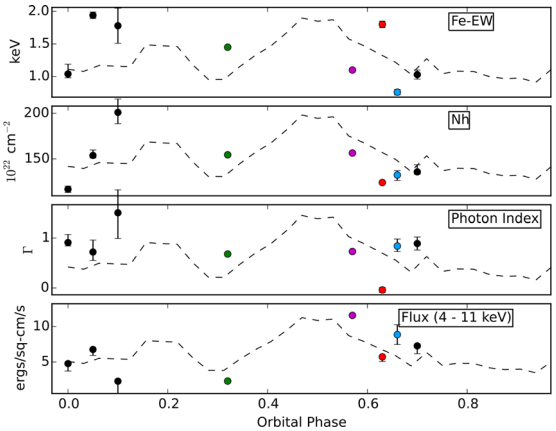

Figure 12. Variation of spectral parameters as a function of the orbital phase. The orbital profile is plotted alongside each figure for reference. *Swift* and *ASCA* data do not have error bars plotted (see Table 3). The colour scheme of Fig. 3 is followed here to distinguish data from different observatories. See online for a colour version of this figure.

and *NuSTAR* shows a clear increase in HR values (by a factor of 2) with increase in luminosity. This indicates a change in spectral parameters causing increase in source hardness with increase in source luminosity. We examined the spectra of *XMM/NuSTAR* observations as a function of the HR values to investigate this.

The source spectra was obtained in three distinct HR levels denoted as high (HR > 5.5), mid (5.5 > HR > 4.0) and low (HR < 4.0). The spectra were extracted as per the steps mentioned in Section 2. To fit the spectra, we first tried a `powerlaw` model with absorption (`phabs`) and emission lines (`gaussian`). This fit indicated the presence of a cut-off at higher energies. To model the cut-off, we used the `highecut` model. We do note that we could have used `cutoffpl` instead. However, we found a large difference between the photon index for data taken below 10 keV (using only *XMM*) and for data taken till 70 keV (using *XMM* and *NuSTAR*, also see Barragán et al. 2009). This difference is much lesser when the `highecut` model is used, thereby enabling comparison of observations with broad-band data and observations with data up to 10 keV. Thus, the spectral model we use consists of an absorption component (`phabs`), a continuum component (`powerlaw` with `highecut`) and three line components (for Fe-Kα, Fe-Kβ and Ni-Kα). The average spectrum for the entire observation fit by this model is shown in Fig. 11.

The best-fitting model incident spectrum for the segments with different HR values are shown in the right-hand panel of Fig. 10. Table 2 lists the parameters obtained from the fitting routine. We note that the continuum parameters harden with increase in source intensity as seen by decrease in Γ values.

Thus, the variation of the broad-band spectrum over a single observation of ∼60 ks duration is mainly related to change in the photon index (and normalization) of the power-law component, which causes related changes in the HR values and line equivalent widths. However, with the other parameters being nearly constant over the course of an observation, we use the average spectrum of the entire observation in order to see if there are any systematic changes of the spectral parameters with the orbital phase.

2.2.3 *Spectral changes over the orbital duration*

As reported in Table 1, there are nine archival observations distributed over various phases of the orbit of this source. Although more *Swift* observations were available, most of them contained too few integrated counts (< 60) to be useful for spectral analysis, owing to the highly absorbed nature of this source. Fig. 3 shows that none of the observations cover either of the two peaks. All the pointed observations lie in the low intensity phase of the orbital profile.

As shown in the bottom panel of Fig. 12, these pointed mode observations do seem to be following the luminosity trends of the BAT folded profile. Thus, we look for correlations between spectral changes in the pointed mode observations and the BAT folded flux profile. In order to look for spectral changes, we extracted the X-ray spectrum for each of the pointed mode observations and modelled the spectrum as mentioned in Section 2.2.2. For observations with data up to 10 keV (*XMM*, *Swift* and *ASCA*), the high-energy cut-off was not used while modelling the data.

We do note that when we used a simple Gaussian model for the three lines, we ignore the effects of a Compton shoulder (as used in Matt & Guainazzi 2003; Ibarra et al. 2007) or the presence of multiple lines of different ionization states (as used in Barragán et al. 2009). As a result of this, although we cannot compare our results for line equivalent widths with these results, we get a simple way to compare all the archival observations in a consistent manner. Secondly, we also note that strong correlations exist between the power-law index (Γ) and the column density ($N_{\rm H}$, see also fig. 1 of

Table 2. Absorption, line and continuum parameters as a function of HR changes in the *XMM/NuSTAR* observation.

Obs	Nh (× 10^{22})	Fe-Kα EW (keV)	Γ	Ecut	Efol	χ^2/dof
HR high	$116.68^{-1.61}_{+1.67}$	$1.86^{-0.12}_{+0.12}$	$-0.42^{-0.09}_{+0.10}$	$7.1^{+0.66}_{-0.19}$	$11.3^{+0.12}_{-0.13}$	421.54/387
HR mid	$123.95^{-1.55}_{+1.58}$	$1.55^{-0.09}_{+0.09}$	$0.07^{-0.10}_{+0.10}$	$7.0^{+0.18}_{-0.29}$	$12.6^{+0.11}_{-0.23}$	460.45/401
HR low	$127.46^{-1.27}_{+1.26}$	$1.93^{-0.19}_{+0.19}$	$0.15^{-0.10}_{+0.11}$	$6.7^{+0.25}_{-0.19}$	$13.2^{+0.22}_{-0.19}$	320.26/348
Avg Spec	$124.10^{-0.63}_{+0.59}$	$1.80^{-0.05}_{+0.05}$	$-0.04^{-0.05}_{+0.05}$	$6.9^{-0.14}_{+0.13}$	$12.4^{-0.09}_{+0.09}$	1009.1/885

Table 3. Spectral parameters obtained from fitting each of the pointed mode observations. Errors are 1σ values.

Observatory	Orb. phase	Nh ($\times 10^{22}$)	Fe-K α EW (keV)	Γ	Flux (4–11 keV) ($\times 10^{-12}$) erg sq-cm^{-1} s^{-1}
XMM	0.00	$116.73^{-3.50}_{+3.48}$	$1.04^{-0.06}_{+0.15}$	$0.91^{-0.07}_{+0.16}$	$4.78^{-1.06}_{+0.04}$
XMM	0.05	$153.83^{-2.83}_{+5.99}$	$1.94^{-0.05}_{+0.05}$	$0.72^{-0.17}_{+.24}$	$6.77^{-0.85}_{+0.02}$
XMM	0.10	$201.05^{-12.33}_{+14.69}$	$1.78^{-0.27}_{+0.27}$	$1.50^{-0.51}_{+0.46}$	$2.29^{-1.73}_{+0.02}$
Swift[a]	0.32	154.50	1.45	0.68	2.31
ASCA[a]	0.57	156.46	1.10	0.73	11.59
XMM-NuSTAR	0.63	$124.10^{-0.63}_{+0.59}$	$1.80^{-0.05}_{+0.05}$	$-0.04^{-0.05}_{+0.05}$	$5.73^{-0.66}_{+0.08}$
Suzaku	0.66	$132.31^{-5.88}_{+4.75}$	$0.76^{-0.04}_{+0.04}$	$0.84^{-0.11}_{+0.14}$	$8.87^{-1.40}_{+1.40}$
XMM	0.70	$135.79^{-2.45}_{+7.73}$	$1.03^{-0.07}_{+0.07}$	$0.89^{-0.13}_{+0.13}$	$7.28^{-1.12}_{+0.12}$

Note. [a]Data has very poor statistics, thereby giving very large errors in *Swift* and *ASCA* parameters. Only the central values are quoted here.

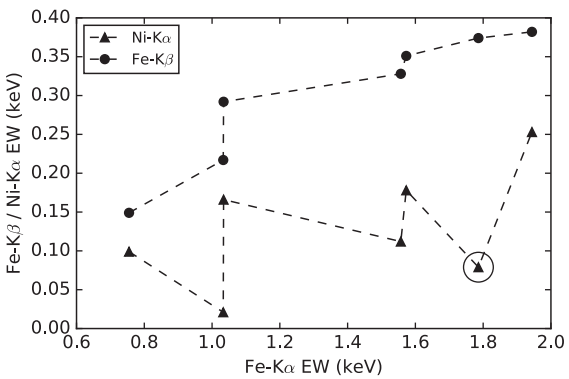

Figure 13. Correlated variations in the Fe-K α and Fe-K β/Ni-K α observations. Circled point indicated observation with the highest column density.

Matt & Guainazzi 2003). This can cause multiple degenerate fits resulting in different local minima. This degeneracy is broken with the availability of broad-band data (as seen in Ibarra et al. 2007; Barragán et al. 2009). Excepting a couple of observations, all our data sets have spectrum only up to 10 keV. For these low-energy observations, we try to consistently get the best-fitting value by checking for other local minima using the `steppar` command. It is noted that Ibarra et al. (2007) do model some of the data sets with additional *INTEGRAL* observations, thereby breaking the degeneracy. We use only the *XMM* observations (<10 keV) for these data sets in order to keep the analysis consistent for all *XMM* observations.

To look for spectral changes, we checked for change in one line parameter (Fe-K α equivalent width), one absorption parameter (column density) and one continuum parameter (photon index) as a function of the orbital phase. These variations are plotted in Fig. 12 and tabulated in Table 3. The fluxes of the two iron lines (Fe-K α, Fe-K β) are correlated with each other as expected. This is shown in the Fig. 13. However, the nickel line variations (triangular points in Fig. 13) do not seem to follow the iron line variations. This, though, could be a result of the very strong absorption present after the Fe-K edge (at ~7.11 keV), which can cause the nickel line to be below detection limits for observations with a large column density. As the lines are largely correlated, we just note the variation in Fe-K α with change in the orbital phase.

The absorption column density remains persistently high ($N_{\rm H} > 10^{24}$ cm^{-2}) through all phases of the orbit. The iron line equivalent width too is seen to be fairly high (>0.7 keV) in all phases of the orbit. The photon index Γ is seen to vary across a single observation, so drawing conclusions from its variation in the average spectrum may not be useful. However, we do note that the obtained photon indices indicate a very hard spectrum with values in the range (−0.1 to 1.5).

Given the limited coverage of different orbital phases by pointed mode observations, it is difficult to draw conclusions from the trends in the parameters. There seems to be an indication of a continuous rise in $N_{\rm H}$ values just before the Secondary Peak is seen. It would be interesting to have more observations to note the variations of these parameters in the Main and Secondary Peaks.

3 DISCUSSION

From the timing analysis of this source, we see that there are two peaks in the orbital folded profile. Based on the spectral and timing observations, we try to speculate upon the reasons behind the formation of two such peaks in the orbital folded profile.

By selecting data points that are flaring in the BAT SOA light curve, we see that the Main Peak corresponds to a phase during which a large number of flares (factor of 10 or greater) are seen as was detected in 2008 Sep. The non-flaring data also has a signature of enhanced emission in the Main and Secondary Peaks. However, the flaring data points have a preference for the orbital phase during which they occur. A possible picture of the accretion process in this binary which could explain all of the above is considered in the following subsection.

3.1 Orbital picture

Using mid-infrared spectroscopic observations, Chaty & Rahoui (2012) inferred IGR J16318−4848 to be a near edge-on binary system with a massive evolved sgB[e] star at the centre of the system. This system was shown to be spectroscopically resolved (in the near-infrared) into three distinct emission regions, viz.

(i) the companion star at ~20 000 K (Rahoui et al. 2008),
(ii) a hot and optically thick rim of puffed up hot dust at ~5000 K at a distance of ~0.8–1.2 au from the companion,
(iii) a warm dust viscous disc like shell with inner disc at ~800 K and extending up to ~5.6 au from the companion.

Given an orbital period of ~80.09 d, we can find where the orbit of the compact object would lie with respect to the companion. Taking the companion mass in the range 25–50 $M_\odot$ (around the likely companion mass of 30 $M_\odot$ reported in Chaty & Rahoui 2012) and the compact object mass in the range of 1.4–10 $M_\odot$ (the typical range of masses of compact objects in our galaxy), we can compute the distance using the expression for mass function of a binary system. The range of mass values assumed gives a range of the separation between the two stars to be in between 0.87 and 1.32 au. For a neutron star compact object (mass in the range 1.4–2.1 $M_\odot$),

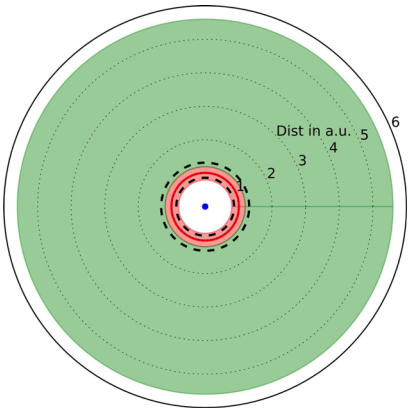

Figure 14. Illustration of the orbit placed in the companion's dust rim as seen from the orbit axis. Blue dot is the companion star, red annulus represents the dust rim and green annulus represents the warm dust disc (Chaty & Rahoui 2012). Black dotted lines represent the minimum and maximum possible values of the orbit semimajor axis. The minimum semimajor axis for a neutron star compact object lies at the dust rim and is not indicated separately here. Distances used to plot the diagram are given in text. Figure assumes a circular orbit. See online text for a colour version of this figure.

the separation comes to be in between 1.0 and 1.32 au. The small change in separation between the black hole and neutron star case is because the separation in a binary system is dependent on the sum of both masses in the binary. In the case of an HMXB system, this separation is mainly governed by the mass of the companion, which is much higher than the compact object mass. This geometry is illustrated in Fig. 14.

Thus, we find that the compact object spends most of its time in either the hot and optically thick dust rim or the warm dust disc of the companion. There might be a few orbital phases when the compact object does enter the cavity in between the companion and the hot dust rim depending on the eccentricity and the actual separation between the stars. However, for an observer the dust rim and the viscous disc always come in the line of sight to the compact object. Such an orbit would be similar to the binary system geometry used to explain the high $N_{\rm H}$ values in CI Cam (see for e.g. fig. 7 of Bartlett et al. 2013, and references therein). It is interesting to note that CI Cam too has a very similar X-ray spectrum to IGR J16318−4848 (in the soft X-rays). These sources could thus be a separate class of X-ray binaries with the compact object enshrouded in the dust rim surrounding an sgB[e] companion.

The two peaks corresponding to phases of enhanced emission can possibly be linked to inhomogeneities in the viscous disc and rim structure surrounding the central sgB[e] star. The large outburst of 2008 Sep possibly caused some re-arrangement of material in the hot dust rim, which leads to a large gap (of 10 orbits) without any detected flare. The re-arranged clumps in the hot dust rim can be the likely cause of the random distribution of flares in the Main Peak after the Sep 2008 outburst.

An interesting point worth noting is the absence of cyclotron resonant scattering features (CRSFs) in the X-ray spectrum of this source. This coupled with the absence of pulsation detections raises questions on the type of compact object. The spectral shape (which is similar to other neutron star HMXBs) and the absence of a radio jet (Filliatre & Chaty 2004) points to a neutron star nature of the compact object. This system could then possibly be a binary with the neutron star poles not crossing our line of sight. Even if the poles do cross our line of sight, smearing due to scattering of X-rays from the surrounding medium may possibly be wiping out signatures of pulsations (Kuster et al. 2005).

4 SUMMARY AND CONCLUSIONS

Our analysis confirms an 80.09 d periodicity in the *Swift* BAT light curve of IGR J16318−4848. We take this to be the orbital period and show the presence of two phases of enhanced X-ray emission in the orbit folded light curve of this source. The 80.09 d orbit places the compact object in this binary system within a rim of hot dusty gas that surrounds the companion sgB[e] star. This enshrouded path of the compact object orbit causes the large observed absorption column in this source. Intermittent flares seen in the source could possibly be due to inhomogeneous sections of the orbit in the hot dust rim. These flares form the Main Peak as seen in the orbit folded light curve.

Further examination of the spectral variability as a function of the orbital phase can give a better understanding of this picture. We believe that an orbit-phase-resolved observational study of the X-ray spectral parameters needs to be carried out to improve our knowledge of this interesting binary system.

ACKNOWLEDGEMENTS

This research has made use of data and software provided by the High Energy Astrophysics Science Archive Research Center (HEASARC), which is a service of the Astrophysics Science Division at NASA/GSFC and the High Energy Astrophysics Division of the Smithsonian Astrophysical Observatory. It is additionally based on observations obtained with *XMM–Newton*, an ESA science mission with instruments and contributions directly funded by ESA Member States and NASA. The research also made use of the *Swift*/BAT transient monitor results provided by the *Swift*/BAT team. We would like to thank all the proposers of the archival observations used in this work. We would also like to thank the anonymous referee for his/her suggestions, which helped improve the manuscript.

REFERENCES

Barragán L., Wilms J., Pottschmidt K., Nowak M. A., Kreykenbohm I., Walter R., Tomsick J. A., 2009, A&A, 508, 1275
Bartlett E. S., Clark J. S., Coe M. J., Garcia M. R., Uttley P., 2013, MNRAS, 429, 1213
Casares J., Negueruela I., Ribó M., Ribas I., Paredes J. M., Herrero A., Simón-Díaz S., 2014, Nature, 505, 378
Chaty S., Rahoui F., 2012, ApJ, 751, 150
Chaty S., Rahoui F., Foellmi C., Tomsick J. A., Rodriguez J., Walter R., 2008, A&A, 484, 783
Courvoisier T. J.-L., Walter R., Rodriguez J., Bouchet L., Lutovinov A. A., 2003, IAU Circ., 8063
Filliatre P., Chaty S., 2004, ApJ, 616, 469
Ibarra A., Matt G., Guainazzi M., Kuulkers E., Jiménez-Bailón E., Rodriguez J., Nicastro F., Walter R., 2007, A&A, 465, 501
Jain C., Paul B., Dutta A., 2009, Res. Astron. Astrophys., 9, 1303
Krimm H. A. et al., 2010, Astron. Telegram, 3051
Krimm H. A. et al., 2013, ApJS, 209, 14
Kuster M., Wilms J., Staubert R., Heindl W. A., Rothschild R. E., Shakura N. I., Postnov K. A., 2005, A&A, 443, 753
Leahy D. A., Darbro W., Elsner R. F., Weisskopf M. C., Kahn S., Sutherland P. G., Grindlay J. E., 1983, ApJ, 266, 160
Matt G., Guainazzi M., 2003, MNRAS, 341, L13
Osaki Y., 1996, PASP, 108, 39
Rahoui F., Chaty S., Lagage P.-O., Pantin E., 2008, A&A, 484, 801
Walter R. et al., 2003, A&A, 411, L427
Walter R., Lutovinov A. A., Bozzo E., Tsygankov S. S., 2015, A&AR, 23, 2

This paper has been typeset from a TEX/LATEX file prepared by the author.